# Construction of a Real-Time Hybrid Simulation Testing Facility and Validation for Offshore Wind Turbine System Behavior under Realistic Wind and Wave Loading Conditions

Qasim Abu-Kassab, S.M.ASCE[1]; Muhannad T. Suleiman, Ph.D., M.ASCE[2]; Safwan Al-Subaihawi, Ph.D., M.ASCE[3]; James M. Ricles, Ph.D., P.E., M.ASCE[4]; Thomas Marullo[5]; Richard Sause, Ph.D., P.E., M.ASCE[6]; Kevin Wyckoff[7]; Liam Magargal[8]; Arindam Banerjee, Ph.D.[9]; Justin W. Jaworski, Ph.D.[10]; and Mohamed Mekkawy, Ph.D., P.E., M.ASCE[11]

[1]Ph.D. Candidate, Dept. of Civil and Environmental Engineering, Lehigh Univ., Bethlehem, PA. Email: qaa219@lehigh.edu
[2]Professor, Dept. of Civil and Environmental Engineering, Lehigh Univ., Bethlehem, PA. Email: mts210@lehigh.edu
[3]Postdoctoral Research Associate, Department of Civil and Environmental Engineering, Lehigh Univ., Bethlehem, PA. Email: swa313@lehigh.edu
[4]Bruce G. Johnston Professor of Structural Engineering, Dept. of Civil and Environmental Engineering, Lehigh Univ., Bethlehem, PA. Email: jmr5@lehigh.edu
[5]Research Scientist and RTMD IT Manager, ATLSS Engineering Research Center, Lehigh Univ., Bethlehem, PA. Email: tmm3@lehigh.edu
[6]Joseph T. Stuart Professor of Structural Engineering, Dept. of Civil and Environmental Engineering, Lehigh Univ., Bethlehem, PA. Email: rs0c@lehigh.edu
[7]Ph.D. Student, Dept. of Mechanical Engineering and Mechanics, Lehigh Univ., Bethlehem, PA. Email: kpw320@lehigh.edu
[8]Ph.D. Student, Dept. of Mechanical Engineering and Mechanics, Lehigh Univ., Bethlehem, PA. Email: lkm322@lehigh.edu
[9]Professor and Chair, Dept. of Mechanical Engineering and Mechanics, Lehigh Univ., Bethlehem, PA. Email: arb612@lehigh.edu
[10]Associate Professor, Dept. of Mechanical Engineering and Mechanics, Lehigh Univ., Bethlehem, PA. Email: jwj213@lehigh.edu
[11]Principal Engineer, Gavin & Doherty Geosolutions. Email: MMekkawy@gdgeo.com



## ABSTRACT

Wind, wave, 1P, and 3P loading subject the offshore wind turbine (OWT) structure to multidirectional long-term cyclic loads that have varying amplitudes, frequencies, and patterns. Therefore, studying the soil-foundation-structure interaction (SFSI) under realistic loading is required to understand the response of the entire OWT during the service life of the structure. This paper presents the establishment and capabilities of a new large-scale multidirectional offshore wind SFSI testing facility at the Advanced Technology for Large Structural Systems (ATLSS) research center at Lehigh University. The new testing facility has unique multidirectional loading capabilities that allow for simultaneous application of realistic wind, wave, gravity loads, and their induced moments at the top of the OWT foundations (i.e., mudline). The capabilities of the new testing facility also include large-scale real-time hybrid simulation (RTHS) testing. These capabilities provide the ability to evaluate the response of the whole OWT structure under loading. In addition to presenting the design, concepts, and

framework of the facility, this paper presents validation results for the RTHS framework of OWTs using small-scale tests. These small-scale RTHS tests are used as a first step to prepare for conducting large-scale RTHS tests.

## INTRODUCTION

OWTs experience cyclic and dynamic loading due to wind, wave, rotor vibrations (i.e., 1P load) and vibrations caused by the blade shadowing effects (2P/3P loads). These loads are complicated in nature and affect the overall behavior of the OWT. OWTs are dynamically sensitive structures since the fundamental frequency is very close to the imposed loading frequencies (Bhattacharya 2019). The fundamental frequency of the structure changes during the life of the OWT depending on the behavior of the structure and the Soil-Foundation Interaction (SFI) under loading. Therefore, understanding the SFSI of the OWT under realistic loading is needed to improve the response of the OWT structure subjected to different environmental and mechanical loading conditions. Researchers have traditionally focused on the response of isolated subsystems comprising OWTs. For example, geotechnical researchers are studying the response of OWT foundations only (e.g., monopile). Many researchers have conducted small-scale experimental tests (e.g., Prasad and Chari 1999, Leblanc et al. 2010, Rathod et al. 2021) and numerical simulations (e.g., Achmus et al. 2009, Ahmed and Hawlader 2016, Cheng et al. 2021) to investigate the effects of the unidirectional lateral static and cyclic loading on the response of the OWT foundation. Other researchers have addressed the effect of misalignment between the wind and the wave loading on the SFI by performing multidirectional small-scale experimental tests (e.g., Nanda et al. 2017, Richards et al. 2020 and 2021) and numerical analysis (e.g., Lovera et al. 2021, Li et al. 2023). However, none of the previous experimental studies considered testing the OWT foundations in larger-scale and under combined wind, wave and gravity loading in addition to their induced moments at the mudline as well as incorporating the response of the whole structure using RTHS. RTHS divides the structure into dynamically coupled substructures; one is defined numerically, while the other is physically tested in the lab. Further details about RTHS are discussed later in this paper.

This paper focuses on the design and the loading capabilities of the new large-scale Multidirectional Offshore Wind SFSI-RTHS Testing Facility that would be used for understanding the behavior of the entire OWT structure. Moreover, RTHS framework of OWTs is presented and validated using small-scale monopile experimental setup.

## MULTIDIRECTIONAL OFFSHORE WIND SFSI-RTHS TESTING FACILITY

The establishment of the new testing facility includes designing and constructing a large soil box with dimensions of 4.6×3.65×3.65 m (length × width × height). The design of the soil box considered the current and future trends in offshore wind energy. ABAQUS/STANDARD was utilized to analyze and design the new soil box allowing for combined application of realistic wind and wave loads, gravity loads and induced moments on the OWT in all three spatial directions (X, Y and Z directions). The following sub-sections are discussing further details of the numerical model used in designing the soil box.

**Soil Box Geometry and Components.** The soil box consists of three main parts: the base grid, the wall panels and the reaction beam-column frame. As shown in Figure 1, The base grid consists of five main W-flange girders connected with sixteen W-flange bracing beams to

support a 25.4 mm thick steel plate. The second part includes a total of ten 12.7 mm thick wall panels stiffened with a grid of 25.4 mm thick steel plates. Eight of these panels have the same dimensions of 3.65×1.8 m and two panels with dimensions of 3.65×0.9 m panels that are used to extend the box length in one direction. The reaction frame has a total of eight columns; four W-flange middle columns connecting the wall panels in the mid spans and four L-shape columns connecting the panels at the corners (see Figure 1). The L-shape corner columns are stiffened with multiple triangular 25.4 mm thick steel plates along their lengths. The middle and corner columns are braced by three rows of W-flanged reaction beams on two sides of the box to be used to apply lateral loads and moments. Also, two opposite middle columns are connected by an overhead W-flange beam to apply axial loading. Figure 1 shows the overall geometry of the soil box and its components and Table 1 summarizes the dimensions of the base girders, wall panels, and reaction beams and columns.

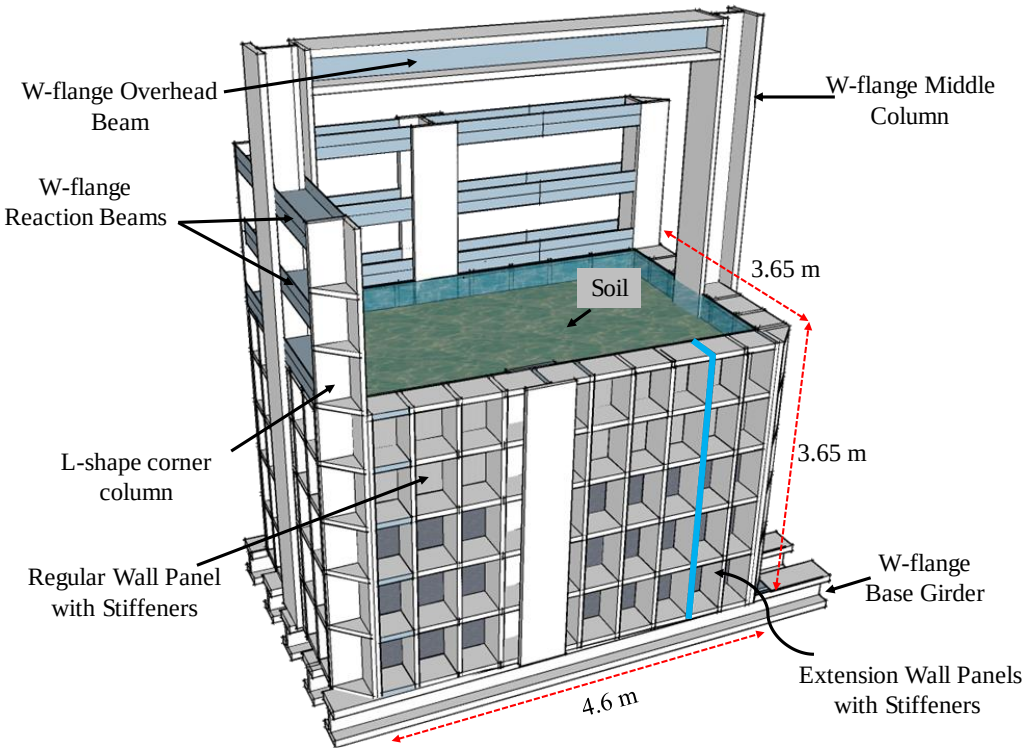


**Figure 1. Soil box geometry and structural components.**

**ABAQUS Model.** The soil box with its reaction frame works as a self-reacting system. SOLIDWORKS was used to build the box numerical model and the model was imported into ABAQUS to analyze the components of the soil box under multidirectional loading. The following sections provide further details about the features used in ABAQUS model and the analysis results for all the critical structural components.

**Material Properties.** Table 2 summarizes all the material properties used in the ABAQUS model. Steel material was used for the soil box components and conservative strength and elastic properties for the concrete floor below the soil box were also defined in the model. For the soil inside the box, Mohr-Coulomb model was used to describe the soil properties.

**Table 1. Soil box structural components sections and dimensions**

| Category | Component | Number | Section | Length (m) | Width (m) |
|---|---|---|---|---|---|
| Base grid | Base bottom plate | 1 | 25.4mm steel plate | 5.65 | 4.3 |
| | Base girders | 5 | W12×96 | 6.4 | - |
| | Base bracing beams | 8<br>8 | W10×45 | 0.9<br>1 | - |
| Wall panels | Regular wall panels | 8 | 13mm steel plate | 3.65 | 1.8 |
| | Extension wall panels | 2 | W/ stiffener's | 3.65 | 0.9 |
| Reaction frame | Middle columns | 1<br>1<br>2 | W14×99 | 3.65<br>6.1<br>7.6 | - |
| | Corner columns | 1<br>3 | L8×8×1 | 3.65<br>6.1 | - |
| | Reaction beam | 12<br>3 | W12×58 | 1.8<br>0.9 | - |
| | Overhead beam | 1 | W12×58 | 3.65 | - |

**Table 2. Material properties in the FE model**

| Material | Strength Parameter | Modulus of Elasticity (MPa) | Density (kg/m$^3$) | Poission's Ratio |
|---|---|---|---|---|
| Steel | ASTM A992<br>$F_y$ = 345 MPa<br>ASTM A36<br>$F_y$ = 248 MPa | 200,000 | 7,855 | 0.3 |
| Concrete | $f'_C$ =28 MPa | 24,856 | 2,490 | 0.15 |
| Soil | Cohesion (C) = 48 kPa<br>Friction angle ($\phi$) = 30° | 15 | 2,041 | 0.4 |

**Boundary Conditions, Components Interactions, and Mesh Size.** Fixed boundary conditions were used at the bottom and the edges of the concrete layer below the soil box. Tie constraints were used between the steel sections to simulate the bolted connections between the steel sections. This type of constraint maintains the rigidity between the structural components. The soil-steel and concrete-steel interactions depend on the frictional and the normal forces that act on the interface between the two materials. ABAQUS provides the option of defining the friction coefficient and the type of normal behavior between the materials. Rabbat et al. (1985)

conducted experimental testing to determine the static friction coefficient ($f_s$) between a steel plate placed on concrete and reported a value of 0.57 for the dry steel-concrete interface. The coefficient of friction between soil and steel varies based on the interface roughness, size and shape of the soil particle and the soil gradation (Han et al. 2018). Han et al. (2018) concluded that rough surfaces increase the interface angle of friction especially when fine sand is used. Based on their results, the critical-state friction angle for 10 different silica sands was between 17.4° and 33.4° (i.e., friction coefficient between 0.31 to ~0.66) using steel surfaces with varying roughness. Saturated fine sand will be used in the soil box and the wall panels were painted with multiple layers of protective epoxy coating that gives the panels a shiny and smooth surface. Therefore, a friction coefficient of 0.35 was used in the model with a hard contact for the normal behavior between the two materials. The FE model used an 8-node brick element for the mesh of all the model components with a mesh size of 76.2 mm for the soil box components and 152.4 mm for the concrete floor below the soil box.

**Loading Conditions.** The reaction frame of the soil box allows for the application of multidirectional loading. The FE model was analyzed under multiple load cases to evaluate the stress path between the different box components. The load cases include: (1) unidirectional lateral load, (2) unidirectional lateral and gravity loads, (3) multidirectional lateral loads, gravity loads and moment. The third load case is the most critical and this paper presents the analysis results for this case only. Figure 2 shows the loads directions in the third load case. It is important to mention that high factored design loads were applied in all load cases. A steel monopile model with a diameter of 254 mm and wall thickness of 5 mm was embedded in the soil inside the box model. To simulate the induced moment from the wind and wave forces at the mudline, coupled non-equal lateral forces (F1 and F2) were applied with a vertical distance (D) as shown in Figure 2. The difference between F1 and F2 is equal to the lateral resultant of aero- and hydro- loads applied on the OWT. F3 represents the dead weight of the OWT at the top of the foundation. The soil box is designed to sustain high loading levels with F1, F2, F3 up to ~ 90, 130 and 45 kN, respectively. F1, F2 and F3 are static forces and applied instantaneously in the FE model. It is worth mentioning that the expected loading levels in the large-scale tests are lower than the design loads (e.g., ~ 5-10 kN in all directions) based on the anticipated scaling ratio between the prototype OWT in the field and the physical model in the lab. However, high loading levels were used in designing the box to: (1) account for the loads associated with large OWTs (e.g., 18 and 24 MW), (2) consider the increase in the wind and wave loads due to the extreme environmental conditions such as storms, and (3) add higher design safety factor especially that the physical monopile model in the soil box will be subjected to cyclic and dynamic loading.

**FE Analysis Results.** Figure 3 presents the deformed shape of the overall system under multidirectional loading in addition to the stress distribution and deflection of the most critical wall panel, middle and corner columns. The maximum stress in the wall panel, middle and corner columns are 32.6 MPa, 117 MPa, and 129 MPa, respectively which is lower than the steel yield strength of 345 MPa. The maximum deflection at the top of the wall panel and the top of the middle and corner columns is 1.2 mm, 10 mm, and 11 mm which has minimal effect on the functionality of the entire soil box and the reaction frame. It is important to mention that lower stresses and deflections are expected under the testing conditions in the soil box since these results are based on high design loads (F1, F2 and F3) of ~90, 130, and 45 kN, respectively.

Based on the FE results, the used steel sections are suitable for the design of the soil box. Detailed structural drawings of the soil box components were developed at ATLSS for

fabrication. Moreover, a new control room was prepared as a part of the new testing facility. The control room includes **MTS FlexTest 100** control system**, Model 6000U Pacific Instrument** Data Acquisition System, **Speedgoat Performance Real-Time System** and multiple monitors with a camera system for recording large-scale **tests.** Figure 4 shows the new large-scale Multidirectional Offshore Wind Soil-Foundation-Structure Interaction RTHS Testing Facility at ATLSS-Lehigh University.

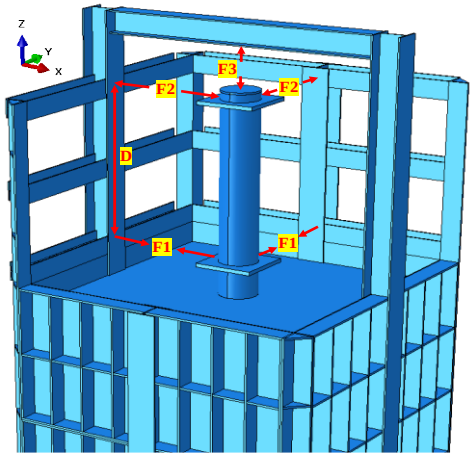


**Figure 2. Applied loads on the reaction frame and the monopile in the FE model.**

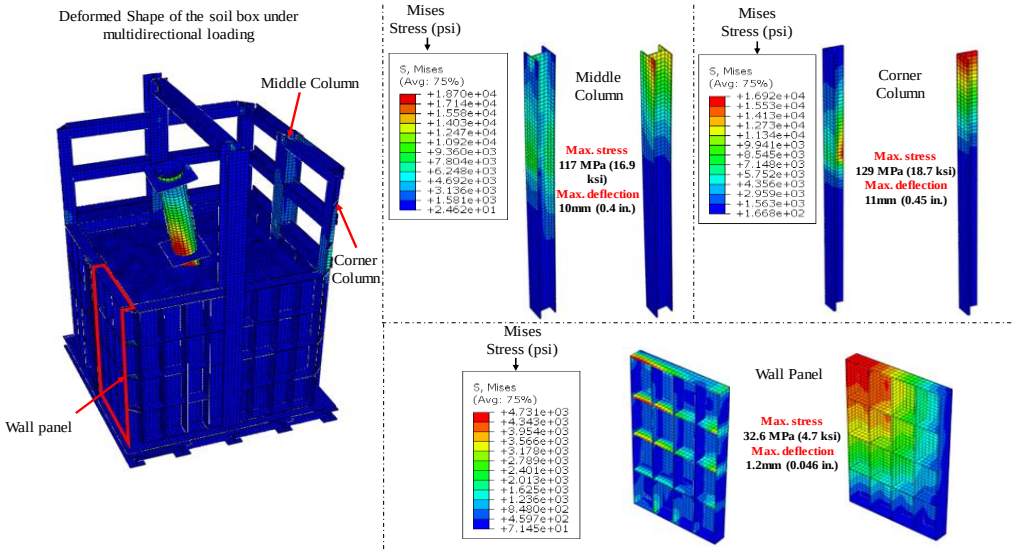


**Figure 3. Mises stress and deflection of the most critical wall panel and columns.**

## REAL-TIME HYBRID SIMULATION (RTHS)

The new testing facility includes developing and implementing RTHS approach that allows for studying the behavior of the entire OWT structure. The RTHS approach divides the OWT into two dynamically coupled subsystems with the compatibility and the dynamic equilibrium maintained at the interface node between the subsystems. One subsystem is modeled numerically

(called the analytical substructure), which includes the superstructure above the mudline in this case. The other subsystem is physically tested in the lab (experimental substructure), which includes the soil-foundation substructure below the mudline in this case. For the analytical substructure, an open-source simulation tool (OpenFAST), developed by the National Renewable Energy Laboratory (NREL), is linked to the RTHS coordinator to determine the hydrodynamic and aerodynamic loads ($F_i^w$ and $F_i^h$) acting on the OWT, along with modeling the dynamics of the electric power generation equipment and associated controller for the OWT. Figure 5 provides a schematic for the RTHS framework to show the data flow between the analytical and the experimental subsystems. To calculate the applied displacement ($u^e_i$) on the experimental substructure at the mudline, an integration for the equations of motion is implemented in the RTHS coordinator. The integration of the equation of motion in the RTHS coordinator includes the hydrodynamic loads ($F^h_i$), interface nodal forces ($F^I_i$), restoring forces from the analytical substructure ($R^a_i$) and the experimental substructure ($R^e_i$) to solve for the analytical ($u^a_i$,$\dot{u}^a_i$) and experimental ($u^e_i$, $\dot{u}^e_i$) displacement and velocity. The restoring forces from the experimental substructure ($R^e_i$) is measured using a load cell. It is important to mention that the integration of the equations of motion in the RTHS coordinator is done for each time step to solve for analytical and experimental displacements and velocities during the simulation time. For further details of the RTHS, the readers are advised to refer to Al-Subaihawi et al. (2023).

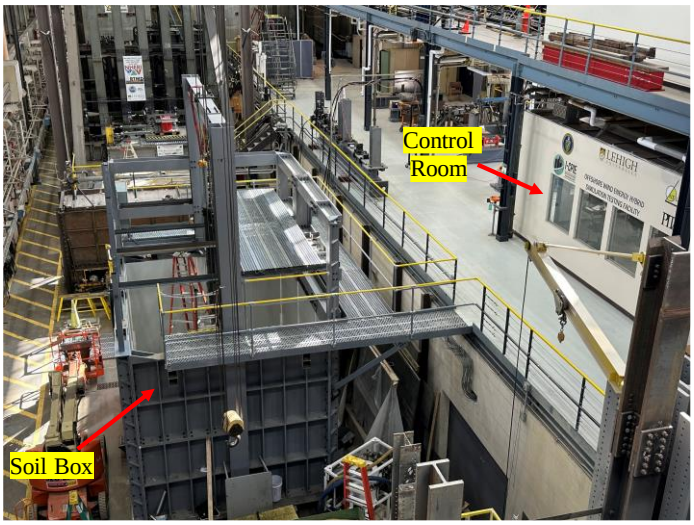


**Figure 4. The New Large-Scale Multidirectional Offshore Wind SFSI-RTHS Testing Facility at ATLSS-Lehigh University.**

**Small-Scale RTHS Testing Setup.** The small-scale setup was used to validate the RTHS framework presented in Figure 5. Validating the RTHS framework does not require using a soil box with dimensions that match the same aspect ratio of the large soil box. Therefore, the small-scale setup includes a soil box with dimensions of 0.9× 0.65×0.75 m. The test specimen is a hollow aluminum pipe pile with a diameter of ~51 mm and embedment length of 580 mm. The pile is embedded in a loose dry silica sand with minimum and maximum dry unit weight of 15.14 kN/m$^3$ and 17.76 kN/m$^3$ obtained according to ASTM D4253-16 and D4254-16. An electric actuator from ULTRAMOTION with a stroke length of 178 mm and a force capacity of 2224 N is connected to a reaction column from one end and to a collar around the pile specimen from the

other end at 200 mm above the sand surface. S-shape load cell from ARTECH with a capacity of 2224 N is connected to the actuator for force measurements and one LVDT from MACRO SENSORS with a stroke length of +/- ~51 mm is connected to the pile at the same elevation of the actuator for displacement measurements. Figure 6 shows the small-scale experimental setup.

**Small-Scale RTHS Validation Tests.** To validate the RTHS for OWTs (see Figure 5), two RTHS small-scale tests were performed under normal and extreme environmental conditions. In the RTHS tests, the 5MW OWT (Jonkman et al. 2009) is used as the reference full-scale model. Myers et al. (2015) provided measured wind and wave data for 50-year normal and extreme hazards at three NOAA measurements locations; Maine, Delaware, and Georgia. The data provided for Maine is used in the RTHS tests. For the test under normal conditions, steady wind and regular wave profiles were used with a wind speed, significant wave height and wave period of 11.4 m/s, 3.66 m and 7.12 sec, respectively. Similar wind and wave profiles were used for the test under extreme conditions but with a wind speed, significant wave height and wave period of 32.9 m/s, 10 m and 11.8 sec.

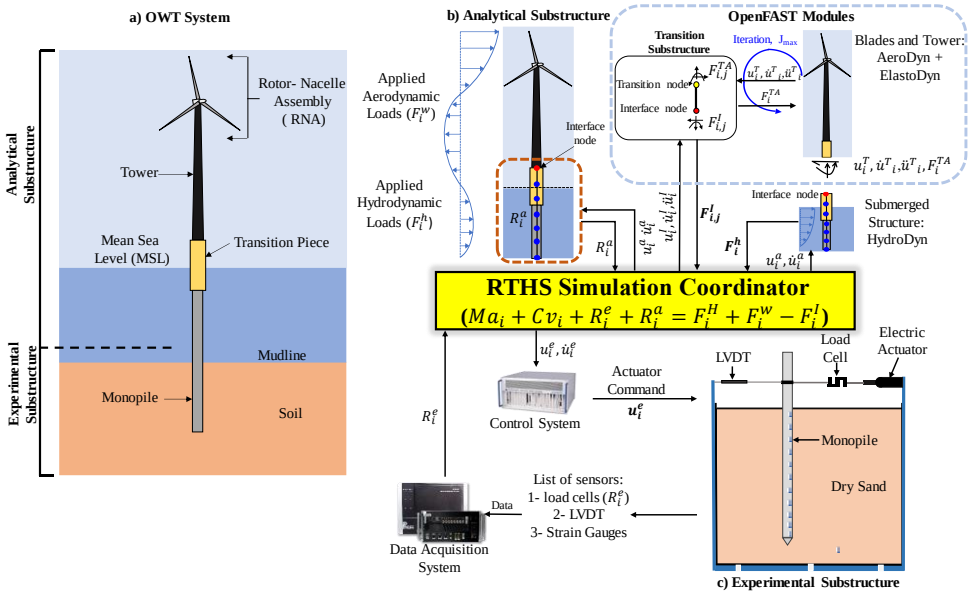


**Figure 5. Real-Time Hybrid Simulation (RTHS) framework for OWTs.**

It is important to mention that the input files and the results in OpenFAST are for the full-scale prototype. Therefore, a length scaling factor (λ) of ~ 120 ((pile diameter) $_{field}$ / (pile diameter) $_{lab}$) was used to scale down the applied displacement on the monopile physical model. Then the restoring forces measured by the load cell was scaled-up by a factor of ($\lambda^2$) and fed back into the RTHS coordinator to solve for the displacement command in the next time step. Figure 7 shows the load-displacement hysteresis and displacement profiles applied on the monopile physical model in both tests. The total simulation time in the RTHS tests is 4000 sec. and the frequency of the wave is the dominant frequency in both tests (0.14 and 0.08 Hz for normal and extreme conditions, respectively). This is equivalent to 560 and 320 loading cycles in the normal and extreme conditions tests, respectively. In RTHS tests, it is important to check the agreement between the target displacement that is calculated in the RTHS coordinator and sent to the actuator, and the measured displacement using external displacement sensor. Figure 7(b) and

(d) show excellent match between the target and measured displacements for both tests with a Normalized Root Mean Square Error (NRMSE) of 0.05% and 0.07% for the normal and extreme conditions tests, respectively. This indicates excellent actuator control was achieved in both RTHS tests. The RTHS results are also used to study a realistic SFSI. For example, the load-displacement hysteresis in Figure 7 (a) and (c) shows that the dry sand is stiffening with number of cycles in both tests, and this could change the fundamental frequency of the entire OWT structure which affects the overall behavior of the structure under wind and wave loading. However, the small-scale tests were performed to validate the RTHS framework only without using appropriate similitude laws to mimic the behavior of the full-scale SFSI. More appropriate similitude laws will be used in the large-scale RTHS testing in the new testing facility.

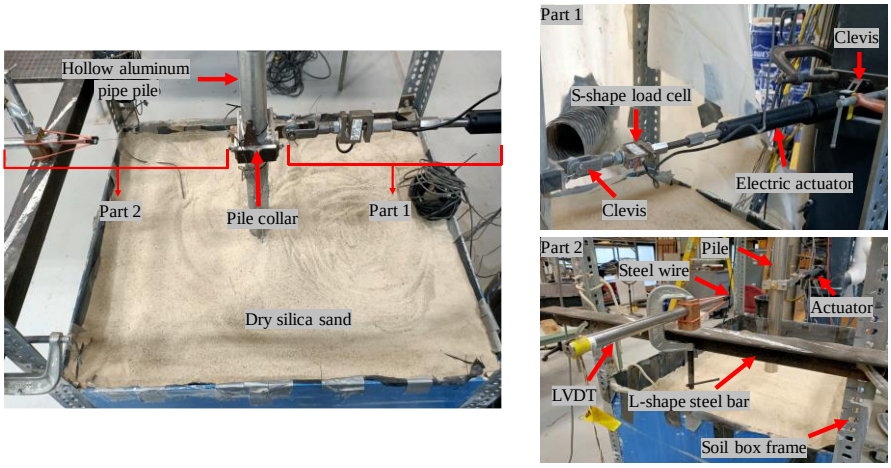


**Figure 6. Small-scale monopile setup for unidirectional lateral loading RTHS test.**

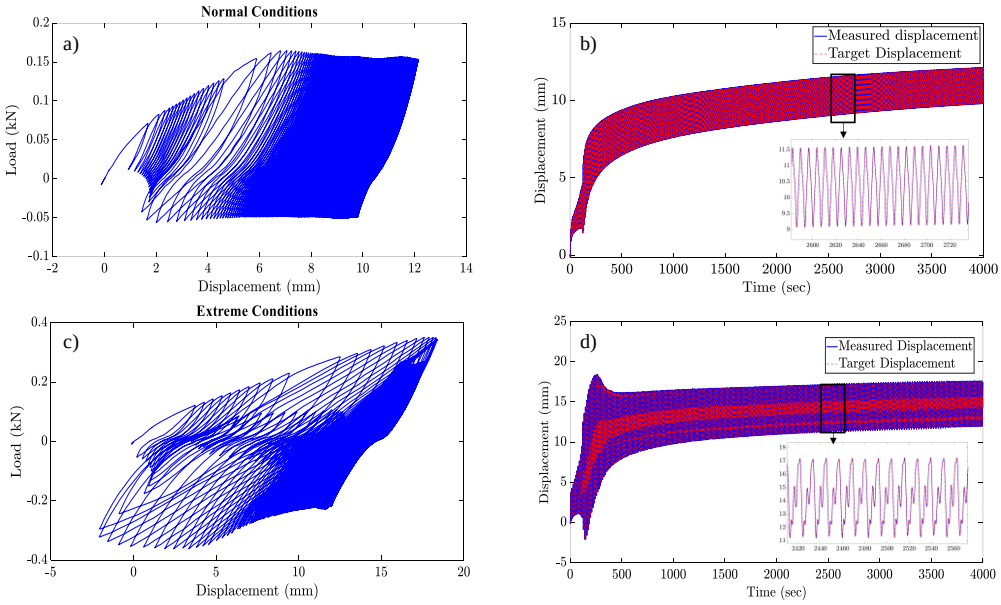


**Figure 7. Load-displacement hysteresis and measured vs target displacement for: (a,b) normal conditions and (c,d) extreme conditions.**

## SUMMARY AND CONCLUSIONS

This paper presents the work conducted to design a new large soil box using ABAQUS. The new soil box is a part of a new large-scale Multidirectional Offshore Wind SFSI-RTHS Testing Facility at Lehigh University. The multidirectional loading capabilities will be used to apply lateral and axial loads and bending moments in X, Y and Z directions to investigate the response of the OWT using RTHS. The RTHS framework is presented and validated using a small-scale test setup as a first step for conducting large-scale RTHS tests.

## ACKNOWLEGEMENT AND DISCLAIMER

This material is based upon work supported by the U.S. Department of Energy's Office of Energy Efficiency and Renewable Energy (EERE) under the Wind Power Technologies Office Award Number DE-EE0008964. The views expressed herein do not necessarily represent the views of the U.S. Department of Energy or the United States Government.

## REFERENCES

Achmus, M., Kuo, Y. S., and Abdel-Rahman, K. (2009). Behavior of monopile foundations under cyclic lateral load. *Computers and Geotechnics*, 36(5), 725-735.

Ahmed, S. S., and Hawlader, B. (2016). Numerical analysis of large-diameter monopiles in dense sand supporting offshore wind turbines. *International Journal of Geomechanics*, 16(5), 04016018.

Al-Subaihawi, S., Ricles, J., Abu-Kassab, Q., Suleiman, M., Sause, R., and Marullo, T. (2023). "Coupled Aero-Hydro-Geotech Real-Time Hybrid Simulation of Offshore Wind Turbine Monopile Structures," *Engineering Structures*, under review for publication.

ASTM. (2016). *Standard Test Methods for Maximum Index Density and Unit Weight of Soils Using a Vibratory Table*. ASTM D4253-16. West Conshohocken, PA: ASTM.

ASTM. (2016). *Standard test methods for minimum index density and unitweight of soils and calculation of relative density*. ASTM D4254-16. West Conshohocken, PA: ASTM.

Bhattacharya, S. (2019). *Design of foundations for offshore wind turbines*. John Wiley & Sons.

Cheng, X., Wang, T., Zhang, J., Liu, Z., and Cheng, W. (2021). Finite element analysis of cyclic lateral responses for large diameter monopiles in clays under different loading patterns. *Computers and Geotechnics*, 134, 104104.

Han, F., Ganju, E., Salgado, R., and Prezzi, M. (2018). Effects of interface roughness, particle geometry, and gradation on the sand–steel interface friction angle. *Journal of Geotechnical and Geoenvironmental Engineering*, 144(12), 04018096.

Jonkman, J., Butterfield, S., Musial, W., and Scott, G. (2009). Definition of a 5-MW reference wind turbine for offshore system development (No. NREL/TP-500-38060). National Renewable Energy Lab. (NREL), Golden, CO (United States).

LeBlanc, C., Houlsby, G. T., and Byrne, B. W. (2010). Response of stiff piles in sand to long-term cyclic lateral loading. *Géotechnique*, 60(2), 79-90.

Li, Z., Liu, H., Hicks, M. A., and Pisanò, F. "Influence of static–cyclic load misalignment on the drained tilting response of offshore monopiles in sand." *Computers and Geotechnics* 156 (2023): 105306.

Lovera, A., Ghabezloo, S., Sulem, J., Randolph, M. F., Kham, M., and Palix, E. (2021). Pile response to multi-directional lateral loading using P–y curves approach. *Géotechnique*, 71(4), 288-298.

Myers, A. T., Arwade, S. R., Valamanesh, V., Hallowell, S., and Carswell, W. (2015). Strength, stiffness, resonance and the design of offshore wind turbine monopiles. *Engineering structures*, 100, 332-341.

Nanda, S., Arthur, I., Sivakumar, V., Donohue, S., Bradshaw, A., Keltai, R., and Glynn, D. (2017). Monopiles subjected to uni-and multi-lateral cyclic loading. *Proceedings of the Institution of Civil Engineers-Geotechnical Engineering*, 170(3), 246-258.

Prasad, Y. V., and Chari, T. R. (1999). Lateral capacity of model rigid piles in cohesionless soils. *Soils and Foundations*, 39(2), 21-29.

Rabbat, B. G., and Russell, H. G. (1985). Friction coefficient of steel on concrete or grout. *Journal of Structural Engineering*, 111(3), 505-515.

Rathod, D., Nigitha, D., and Krishnanunni, K. T. (2021). Experimental investigation of the behavior of monopile under asymmetric two-way cyclic lateral loads. *International Journal of Geomechanics*, 21(3), 06021001.

Richards, I. A., Byrne, B. W., and Houlsby, G. T. (2020). Monopile rotation under complex cyclic lateral loading in sand. *Géotechnique*, 70(10), 916-930.

Richards, I. A., Bransby, M. F., Byrne, B. W., Gaudin, C., and Houlsby, G. T. (2021). Effect of stress level on response of model monopile to cyclic lateral loading in sand. *Journal of Geotechnical and Geoenvironmental Engineering*, 147(3), 04021002.